Royal Norwegian Council
for Scientific and Industrial Research
(NTNF)

NORSAR

NORSAR Scientific Report No. 1-92/93

Semiannual Technical Summary

1 April — 30 September 1992

Kjeller, November 1992

7.2 Initial processing results from the Apatity small-aperture array

During the fall of 1992, a new regional array was installed near the town of Apatity on the Kola Peninsula (see Section 7.1). Figs. 7.1.1 and 7.1.2 show the location of this array and Fig. 7.1.3 shows the array geometry.

In the following we report on some initial results from analyzing data from the new array. It is emphasized that these results are preliminary, since the available data cover only a few weeks. Thus a more comprehensive assessment must await the collection of data over a longer time span.

Noise spectra

Fig. 7.2.1a shows an example of corrected noise spectra for the 9 vertical elements of the Apatity array, taken at 00.00 hours (GMT) on day 345, 1992. For comparison, the ARCESS spectra for the same number of channels and taken at the same time are shown in Fig. 7.2.1b. From these figures, it is seen that the Apatity array has a higher noise level than ARCESS at frequencies above 2 Hz, whereas the noise levels are similar at lower frequencies.

The higher noise level at Apatity above 2 Hz is not unexpected, taking into account the higher level of industrial activity in this region. On the other hand, the noise level at the Apatity array site is considerably lower than that of the APA station situated in the town of Apatity (see NORSAR Sci. Rep. 1-91/92).

Fig. 7.2.2a shows 24 uncorrected noise spectra, taken hourly between 00.00 GMT and 23.00 GMT on day 344 for the Apatity array (instrument A0Z). For comparison, a similar set of NORESS spectra is shown in Fig. 7.2.2b. The range of variability is similar for the two sites, with the highest noise levels corresponding to local daytime.

Noise suppression

Previous studies have shown that regional arrays are very effective in suppressing seismic noise, thus providing gains that are often of the order of $\sqrt{N}$, or sometimes even in excess of this value (N being the number of sensors). Such better than $\sqrt{N}$ suppression occurs when particular subgeometries are chosen, enhancing the suppression of noise at certain frequencies. As a first check on the capabilities of the Apatity array in this regard, we have computed noise suppression curves and compared with corresponding results from NORESS.

We calculate an uncorrected power density spectrum first by prewhitening 60 seconds of data. Then we estimate the autocorrelation for 6 partially overlapping windows (window length 12 seconds), and compute power density spectra from the average autocorrelation, with compensation for the prewhitening filter.

An average spectrum is obtained by averaging the 9 individual channel spectra for the array. The averaging is done after a logarithmic transform of the spectra, and the standard

deviation for each frequency point is calculated. Each spectrum is pointwise compared to the average spectrum. If a value is outside 1.5 standard deviation from the mean value, the point is considered an outlier. If a single channel spectrum has more than 60% outliers, the spectrum is excluded and a new average spectrum is estimated. A beam is calculated using only those channels for which the spectrum was accepted. The suppression is then the beam spectrum divided by the average spectrum.

It should be noted that calculating suppression using a beam with all 9 elements compared to using only "accepted" channels makes little difference in practice. When calculating noise suppression the most stable results are obtained by dividing the beam spectrum with the average spectrum.

Fig. 7.2.3a shows noise suppression in the frequency range 0-20 Hz for an infinite-velocity beam (no time delays) for the Apatity array. There are 24 samples, taken hourly on day 344, 1992. For comparison, a corresponding plot for the 9-element NORESS B-ring array (A0Z, A1-3, B1-5) is shown in Fig. 7.2.3b. The $\sqrt{N}$ level is about -9.5 dB, and the general impression is that the Apatity array is at least as efficient in suppressing noise as the corresponding NORESS subgeometry. Between 1 and 5 Hz, the Apatity array has higher noise suppression than the NORESS B-ring geometry, and we attribute this to the slightly larger Apatity array aperture. Above 5 Hz, the two configurations are similar. At a frequency near 4 Hz, there is significantly better than $\sqrt{N}$ noise suppression for the Apatity array. In summary, it appears that the spatial noise characteristics at Apatity are similar to those found in other areas of Fennoscandia and the Baltic Shield.

Detection processing

Since the array was installed, the Apatity data have been subjected to continuous on-line detection processing (DP) at NORSAR using the detection algorithm described by Mykkeltveit and Bungum (1984). The initial beam deployment is shown in Table 7.2.1. At an early stage, the Apatity detection lists were incorporated into the Generalized Beamforming (GBF) process (Ringdal and Kværna, 1989) , which has been in automatic operation at NORSAR for nearly 3 years. It is noteworthy that both the DP and GBF could be implemented for the new array with success even without any special tailoring of parameter values and algorithms.

As an example of a regional seismic event recorded and processed using Apatity data, we show here results for a presumed mining explosion in the Kola Peninsula west of the array. This event is from an area different than the Khibiny Massif where most such explosions take place.

Fig. 7.2.4 shows B-ring seismograms for this event. Note the very clear Rg phase, which indicates a shallow source. The detector output, and the solution provided by the GBF algorithm, are shown in Table 7.2.2. A total of 10 phases from the four regional arrays in Fennoscandia have been associated with this event. The estimated magnitude (M_L) is 2.53.

Frequency-wavenumber analysis

Frequency-wavenumber solutions for the three phases Pg, Lg and Rg are shown in Fig. 7.2.5a-c. In spite of the small aperture of the array, the peaks in the F-K diagram are well-defined: typically the highest side lobe is at least 6 dB below the main peak in the F-K plot. Analysis of many events has shown that in particular the array gives a very stable determination of slowness and azimuth for the Rg phase in spite of the broad peak in the F-K diagram. It is remarkable how well an array of only 1 km diameter can resolve these low-frequency dispersive waves.

From Fig. 7.2.5 we note that the phase velocities of each of the three phases are consistent with the phase type; the Rg phase having the slowest velocity. The estimated azimuths are also consistent, with a few degrees' difference only.

Teleseismic events

An example of a small teleseismic recording is shown in Fig. 7.2.6. There is clearly a significant SNR gain on the array beam, and this supports the previous statements on noise suppression. Naturally, the gain at teleseismic signal frequencies for the Apatity array will be lower than for the full-scale NORESS, ARCESS and GERESS regional arrays. Nevertheless, for areas of favorable signal focusing effects, the small Apatity array may still show excellent teleseismic detection, and many examples of this have been observed.

In conclusion, our preliminary analysis indicates that the Apatity array will be an important supplement to the seismic array network in Northern Europe, both for regional and teleseismic event analysis. Its inclusion into the Intelligent Monitoring System (IMS) will in particular serve to improve the location precision and source characterization of the large number of seismic events in the Kola Peninsula and adjacent areas.

F. Ringdal
J. Fyen

References

Mykkeltveit, S. and H. Bungum (1984): Processing of regional events using data from small-aperture arrays, Bull. Seism. Soc. Am., 74, 2313-2333.

Ringdal, F. and T. Kværna (1989): A multi-channel processing approach to real-time network detection, phase association and threshold monitoring, Bull. Seism. Soc. Am., 79, 1927-1940.

BEAM	Velocity	Azim	Filter band	Thre	N	Configuration
A011	99999.9	0.0	0.5 - 1.5	4.40	6	A0B
A021	99999.9	0.0	1.0 - 3.0	4.40	6	A0B
A031	99999.9	0.0	1.5 - 3.5	4.40	6	A0B
A032	11.0	30.0	1.5 - 3.5	4.40	6	A0B
A033	11.0	90.0	1.5 - 3.5	4.40	6	A0B
A034	11.0	150.0	1.5 - 3.5	4.40	6	A0B
A035	11.0	210.0	1.5 - 3.5	4.40	6	A0B
A036	11.0	270.0	1.5 - 3.5	4.40	6	A0B
A037	11.0	330.0	1.5 - 3.5	4.40	6	A0B
A038	15.0	80.0	1.5 - 3.5	3.90	6	A0B
A039	10.0	20.0	1.5 - 3.5	3.90	6	A0B
A041	99999.9	0.0	2.0 - 4.0	4.40	9	A0AB
A042	10.2	30.0	2.0 - 4.0	4.40	9	A0AB
A043	10.2	90.0	2.0 - 4.0	4.40	9	A0AB
A044	10.2	150.0	2.0 - 4.0	4.40	9	A0AB
A045	10.2	210.0	2.0 - 4.0	4.40	9	A0AB
A046	10.2	270.0	2.0 - 4.0	4.40	9	A0AB
A047	10.2	330.0	2.0 - 4.0	4.40	9	A0AB
A048	15.0	80.0	2.0 - 4.0	3.90	9	A0AB
A049	10.0	20.0	2.0 - 4.0	3.90	9	A0AB
A051	99999.9	0.0	2.5 - 4.5	4.40	9	A0AB
A052	8.9	30.0	2.5 - 4.5	4.40	9	A0AB
A053	8.9	90.0	2.5 - 4.5	4.40	9	A0AB
A054	8.9	150.0	2.5 - 4.5	4.40	9	A0AB
A055	8.9	210.0	2.5 - 4.5	4.40	9	A0AB
A056	8.9	270.0	2.5 - 4.5	4.40	9	A0AB
A057	8.9	330.0	2.5 - 4.5	4.40	9	A0AB
A058	15.0	80.0	2.5 - 4.5	3.90	9	A0AB
A061	99999.9	0.0	3.0 - 5.0	4.40	9	A0AB
A062	10.5	30.0	3.0 - 5.0	4.40	9	A0AB
A063	10.5	90.0	3.0 - 5.0	4.40	9	A0AB
A064	10.5	150.0	3.0 - 5.0	4.40	9	A0AB
A065	10.5	210.0	3.0 - 5.0	4.40	9	A0AB
A066	10.5	270.0	3.0 - 5.0	4.40	9	A0AB
A067	10.5	330.0	3.0 - 5.0	4.40	9	A0AB
A068	15.0	80.0	3.0 - 5.0	3.90	9	A0AB
A071	99999.9	0.0	3.5 - 5.5	4.40	9	A0AB
A072	11.1	30.0	3.5 - 5.5	4.40	9	A0AB
A073	11.1	90.0	3.5 - 5.5	4.40	9	A0AB
A074	11.1	150.0	3.5 - 5.5	4.40	9	A0AB
A075	11.1	210.0	3.5 - 5.5	4.40	9	A0AB
A076	11.1	270.0	3.5 - 5.5	4.40	9	A0AB
A077	11.1	330.0	3.5 - 5.5	4.40	9	A0AB

Table 7.2.1. Apatity beam table, valid from 1992-274 (1 October 1992). The table shows the name of the beam, velocity (km/sec), azimuth (degrees), filter band (Hz), STA/LTA threshold, and configuration. The configuration is described with number of sensors and a configuration code. Here, A0AB means center A0 SPZ plus A-ring plus B-ring, and A0B means A0 SPZ plus B-ring. The designator (alone) A0 means three-component 80 Hz data from A0. AH01 - AH04 are three-component horizontal beams using the A0 high-frequency system. AI01 - AI06 are incoherent beams using SPZ channels only. (Page 1 of 2)

BEAM	Velocity	Azim	Filter band	Thre	N	Configuration
A081	99999.9	0.0	4.0 - 8.0	4.40	9	A0AB
A082	9.5	30.0	4.0 - 8.0	4.40	9	A0AB
A083	9.5	90.0	4.0 - 8.0	4.40	9	A0AB
A084	9.5	150.0	4.0 - 8.0	4.40	9	A0AB
A085	9.5	210.0	4.0 - 8.0	4.40	9	A0AB
A086	9.5	270.0	4.0 - 8.0	4.40	9	A0AB
A087	9.5	330.0	4.0 - 8.0	4.40	9	A0AB
A091	99999.9	0.0	5.0 - 10.0	4.90	9	A0AB
A092	10.5	30.0	5.0 - 10.0	4.90	9	A0AB
A093	10.5	90.0	5.0 - 10.0	4.90	9	A0AB
A094	10.5	150.0	5.0 - 10.0	4.90	9	A0AB
A095	10.5	210.0	5.0 - 10.0	4.90	9	A0AB
A096	10.5	270.0	5.0 - 10.0	4.90	9	A0AB
A097	10.5	330.0	5.0 - 10.0	4.90	9	A0AB
A101	99999.9	0.0	8.0 - 16.0	4.90	9	A0AB
A102	9.9	30.0	8.0 - 16.0	4.90	9	A0AB
A103	9.9	90.0	8.0 - 16.0	4.90	9	A0AB
A104	9.9	150.0	8.0 - 16.0	4.90	9	A0AB
A105	9.9	210.0	8.0 - 16.0	4.90	9	A0AB
A106	9.9	270.0	8.0 - 16.0	4.90	9	A0AB
A107	9.9	330.0	8.0 - 16.0	4.90	9	A0AB
A201	99999.9	0.0	1.0 - 3.0	4.00	6	A0B
A207	99999.9	0.0	8.0 - 16.0	4.50	6	A0B
A254	99999.9	0.0	2.0 - 4.0	4.00	6	A0B
A282	99999.9	0.0	4.0 - 8.0	4.00	6	A0B
A310	99999.9	0.0	1.0 - 2.0	2.50	6	A0B
A312	99999.9	0.0	2.0 - 4.0	2.40	6	A0B
AH01	99999.9	0.0	2.0 - 4.0	2.80	3	A0
AH02	99999.9	0.0	3.5 - 5.5	2.80	3	A0
AH03	99999.9	0.0	5.0 - 10.0	2.80	3	A0
AH04	99999.9	0.0	8.0 - 16.0	2.80	3	A0
AI01	99999.9	0.0	0.5 - 1.5	2.90	6	A0B
AI02	99999.9	0.0	1.0 - 2.0	2.90	6	A0B
AI03	99999.9	0.0	1.5 - 2.5	2.90	6	A0B
AI04	99999.9	0.0	2.0 - 4.0	2.50	6	A0B
AI05	99999.9	0.0	3.5 - 5.5	2.50	6	A0B
AI06	99999.9	0.0	5.0 - 10.0	2.70	6	A0B

Table 7.2.1 (cont.) (Page 2 of 2)

Origin time	Lat	Lon	Azres	Timres	Wres	Nphase	Ntot	Nsta	Netmag
1992-298:11.18.12.0	67.45	30.50	6.13	1.87	3.40	10	22	4	2.53

Sta	Dist	Az	Ph	Time	Tres	Azim	Ares	Vel	Snr	Amp	Freq	Fkq	Pol	Arid	Mag
APA	107.7	262.2	Pg	11.18.29.1	-0.3	267.7	5.5	6.9	285.5	6816.3	6.10	2	1	15222	
APA	107.7	262.2	p	11.18.30.7		269.4	7.2	8.9	18.6	318.8	2.12	1	1	15223	
APA	107.7	262.2	p	11.18.36.7		254.2	-8.0	7.8	7.1	934.0	3.64	1		15224	
APA	107.7	262.2	s	11.18.40.1		276.7	14.5	4.3	3.0	4265.9	3.62	1		15225	
APA	107.7	262.2	Lg	11.18.41.3	-0.9	271.1	8.9	3.7	12.3	12857.0	4.96	2		15226	1.85
APA	107.7	262.2	s	11.18.43.0		275.3	13.1	4.0	5.5	1670.5	2.03	1	-2	15227	
APA	107.7	262.2	s	11.18.45.5		273.3	11.1	4.3	154.9	5927.3	1.54	1		15228	
APA	107.7	262.2	s	11.18.47.8		282.6	20.4	3.9	108.2	36857.6	1.09	1	-3	15229	2.80
APA	107.7	262.2	Rg	11.18.52.1	3.6	278.5	16.3	3.2	7.1	7395.9	2.04	1	-3	15231	
ARC	309.6	136.3	Pn	11.18.55.6	-2.0	136.0	-0.3	7.3	576.2	8820.1	5.24	1	1	985943	
ARC	309.6	136.3	p	11.19.03.4		131.9	-4.4	7.0	7.6	2731.6	4.77	2		985945	
ARC	309.6	136.3	p	11.19.18.1		134.0	-2.3	6.8	2.8	1038.3	2.57	1	-1	985947	
ARC	309.6	136.3	Sn	11.19.27.2	-7.3	134.3	-2.0	5.1	3.5	2547.7	2.07	1		985948	1.67
ARC	309.6	136.3	s	11.19.32.0		130.3	-6.0	3.8	12.9	10251.3	2.08	1	-2	985950	2.27
ARC	309.6	136.3	Lg	11.19.37.6	-1.0	125.2	-11.1	3.1	4.0	7980.2	2.09	2		985952	2.16
ARC	309.6	136.3	s	11.19.41.4		136.4	0.1	4.8	4.3	10954.3	2.67	1		985953	
FIN	703.3	15.7	Pn	11.19.46.8	1.1	25.8	10.1	9.4	26.9	222.5	4.61	2	1	985942	
FIN	703.3	15.7	p	11.19.58.6		15.9	0.2	8.1	3.2	118.8	4.48	2	1	985944	
FIN	703.3	15.7	Lg	11.21.29.1	0.3	19.8	4.1	4.1	12.6	594.6	2.13	1		985957	2.49
FIN	703.3	15.7	s	11.21.35.3		21.7	6.0	4.6	5.8	720.1	2.58	1		985959	2.59
NRS	1182.9	42.7	Pn	11.20.42.7	-1.3	44.1	1.4	8.8	18.3	412.0	3.77	1	1	985949	
NRS	1182.9	42.7	Lg	11.23.43.9	1.0	41.1	-1.6	3.8	3.5	1141.4	1.36	1	-3	985958	2.45

Table 7.2.2. Automatic results from the on-line generalized beamforming process at NORSAR for the event described in the text. The upper two lines give estimated source parameters and residuals. The phase list shows the individual detections that have been associated with this event from the four arrays Apatity, ARCESS, FINESA and NORESS, and gives some detection parameters. Time residual (T_{res}) is only specified for the phases that have been used to define the event (10 out of 22 total associated phases).

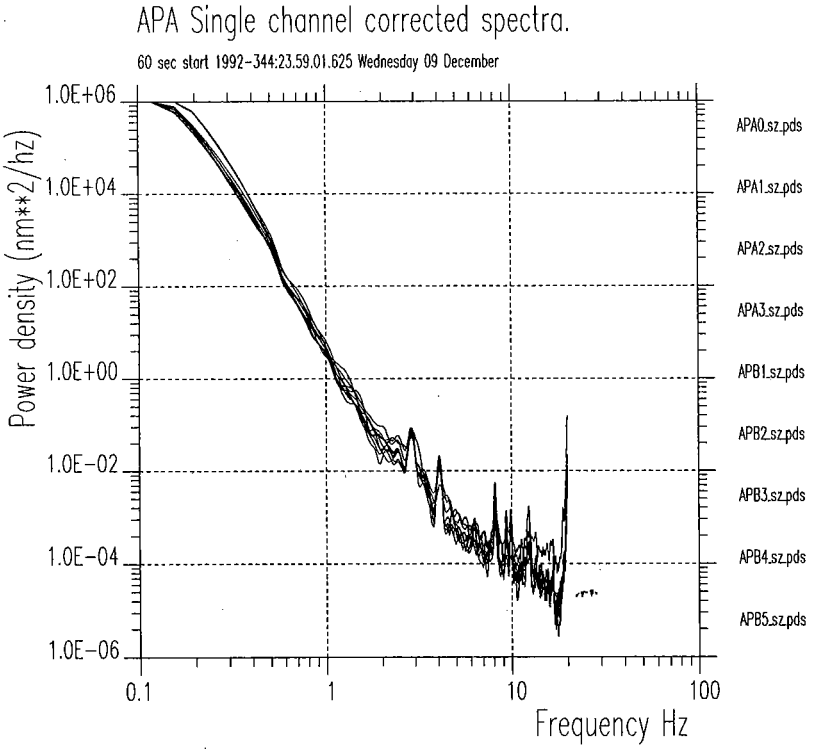

Fig. 7.2.1a. Noise spectra corrected for system response for the Apatity array for 9 vertical channels at A0, the A-ring and the B-ring. The spectra are based on one minute of data at 00.00 hours GMT on day 345, 1992. The power density is in nm^2/Hz.

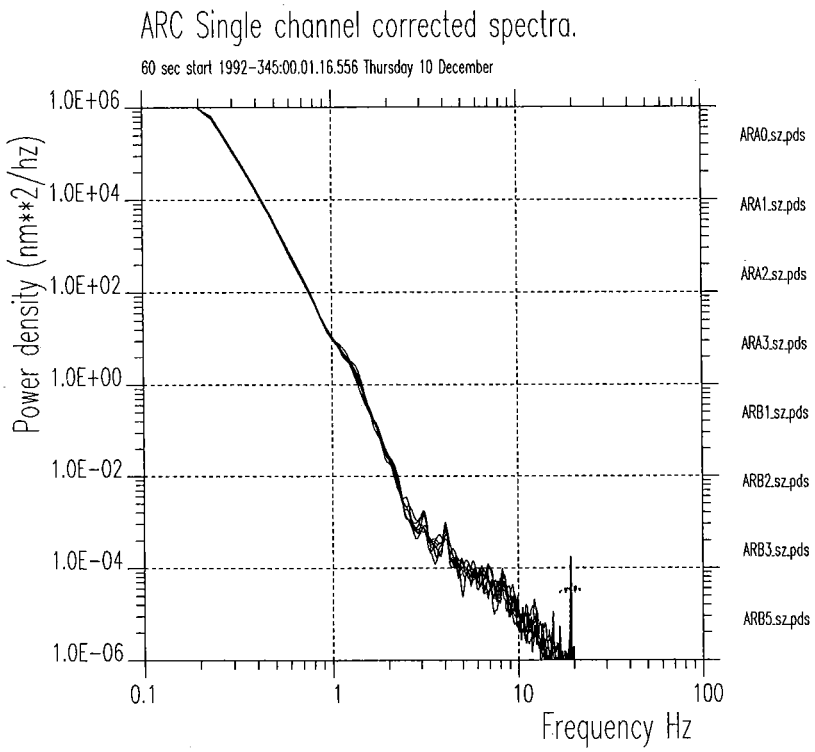

Fig. 7.2.1b. Same as Fig. 7.2.1a, but for ARCESS data (A0, A-ring, B-ring) taken at 00.00 hours GMT on day 345, 1992.

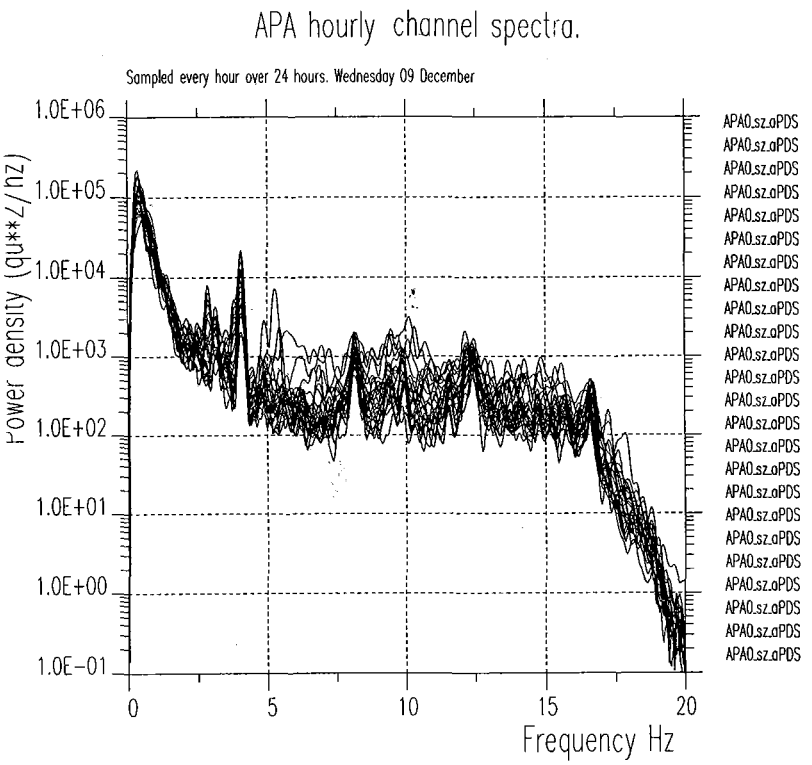

Fig. 7.2.2a. Uncorrected noise spectra for the Apatity array for 24 one-minute intervals taken hourly between 00.00 and 23.00 hours GMT on day 344, 1992. Each spectrum represents data from the A0 SPZ seismometer.

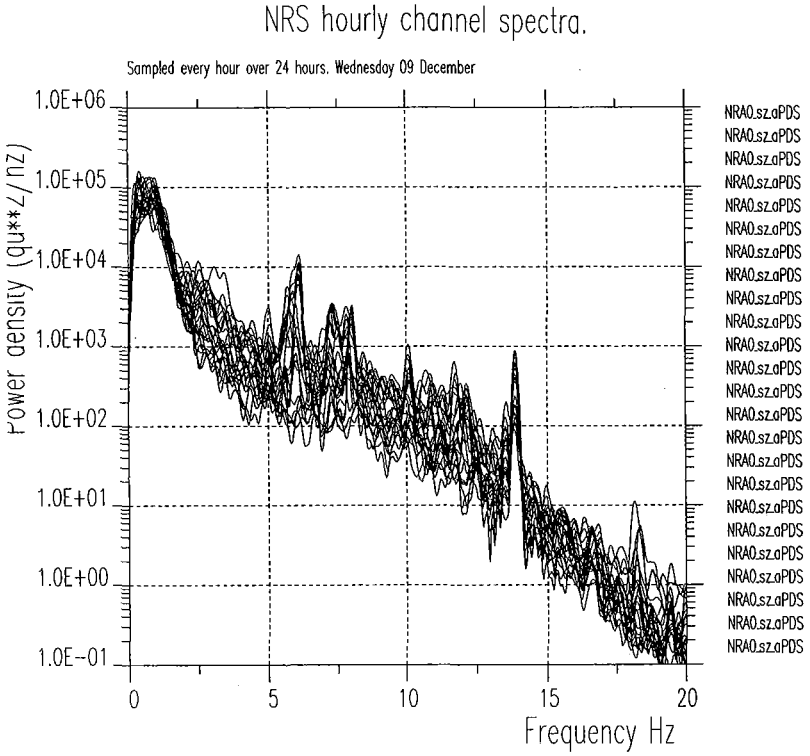

Fig. 7.2.2b. Same as Fig. 7.2.2a but for NORESS data (A0 SPZ seismometer) taken hourly between 00.00 and 23.00 hours GMT on day 344, 1992.

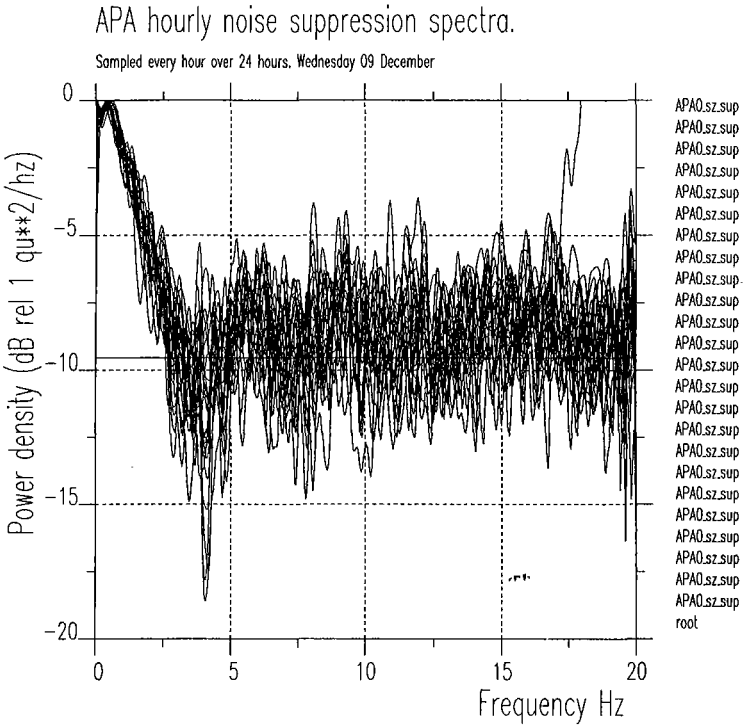

Fig. 7.2.3a. Apatity array noise suppression by beamforming for the geometry comprising A0, A- and B-ring SPZ sensors. To produce these curves, an infinite-velocity beam is formed and the spectrum for this beam is divided by the average of the single sensor spectra. The 24 curves result from one minute of data taken hourly between 00.00 and 23.00 hours GMT on day 344, 1992. The horizontal line at -9.5 dB represents $\sqrt{N}$ suppression for 9 sensors.

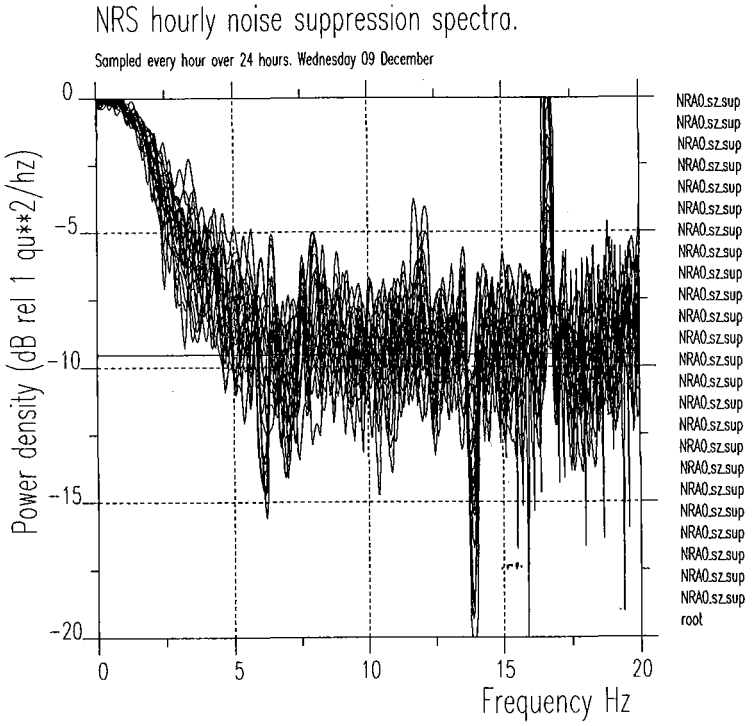

Fig. 7.2.3b. Same as Fig. 7.2.3a but for the 9-element sub-geometry of NORESS consisting of A0, the A- and B-rings.

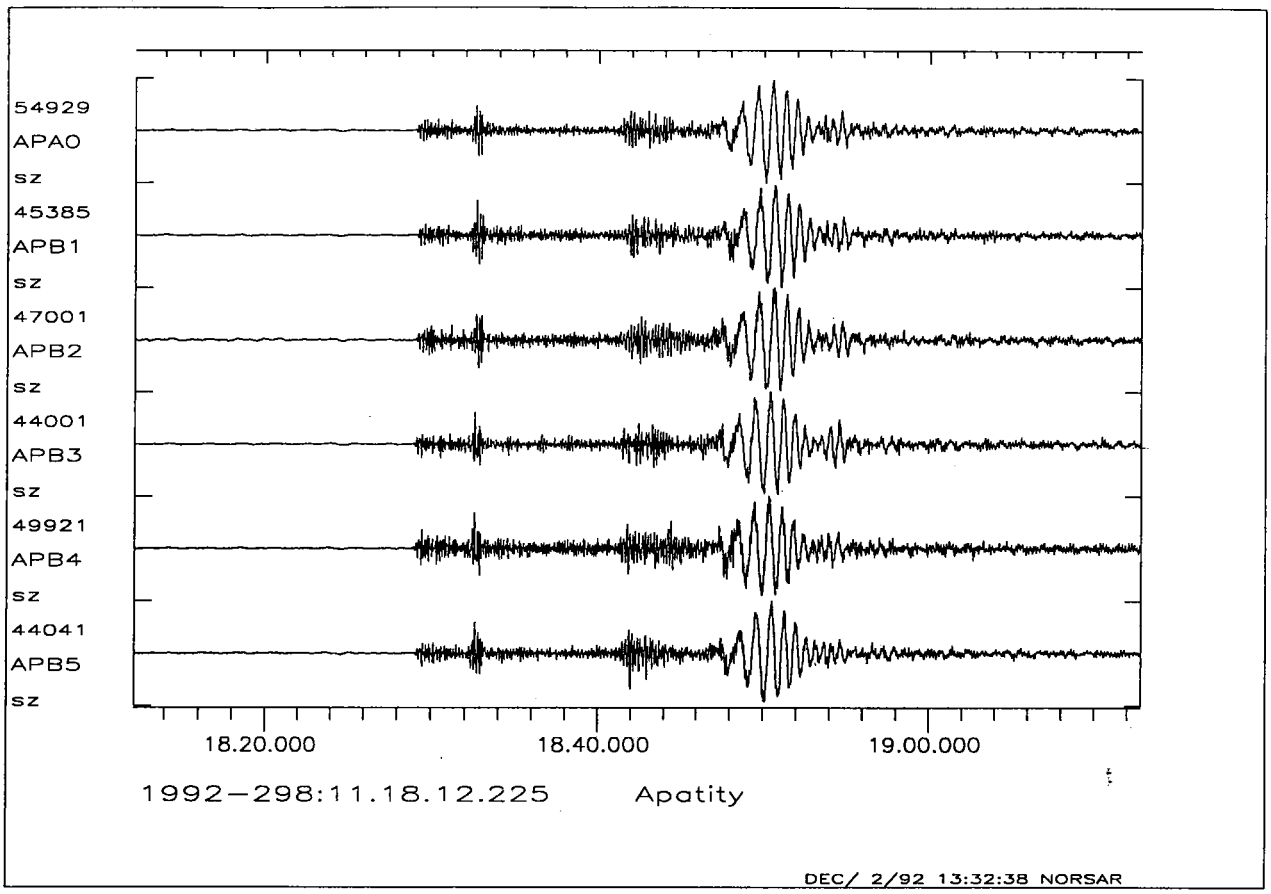

Fig. 7.2.4. Plot of individual APA SPZ channels for the presumed mining explosion discussed in the text (see Table 7.2.2). Note the very prominent Rg phase, indicating a shallow origin.

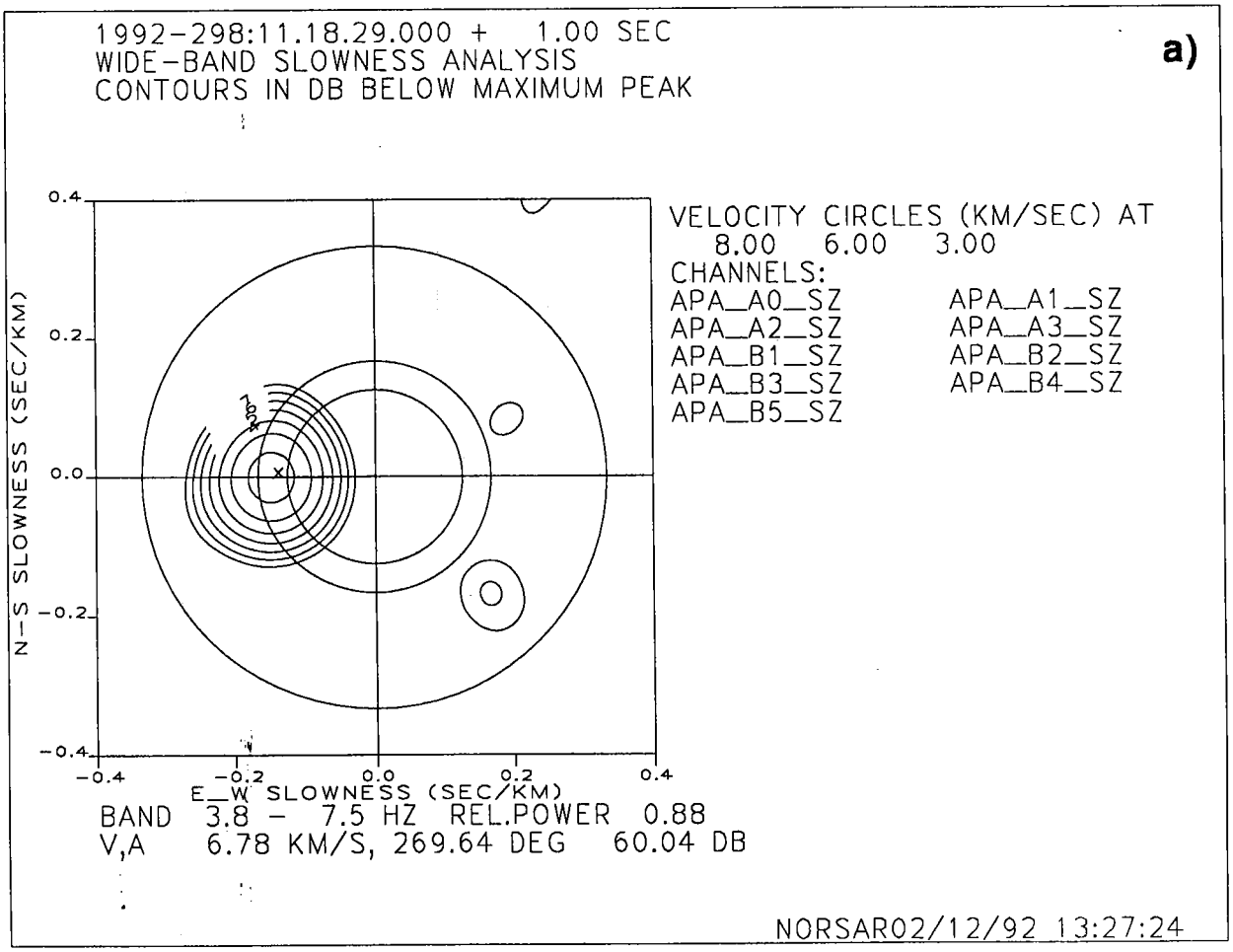

Fig. 7.2.5. Broadband F-K analysis results for the P, Lg and Rg phases of the event shown in Fig. 7.2.4. The figure shows a) the Pg phase, b) the Lg phase and c) the Rg phase. The three velocity circles correspond to 8, 6 and 3 km/s. (Page 1 of 3).

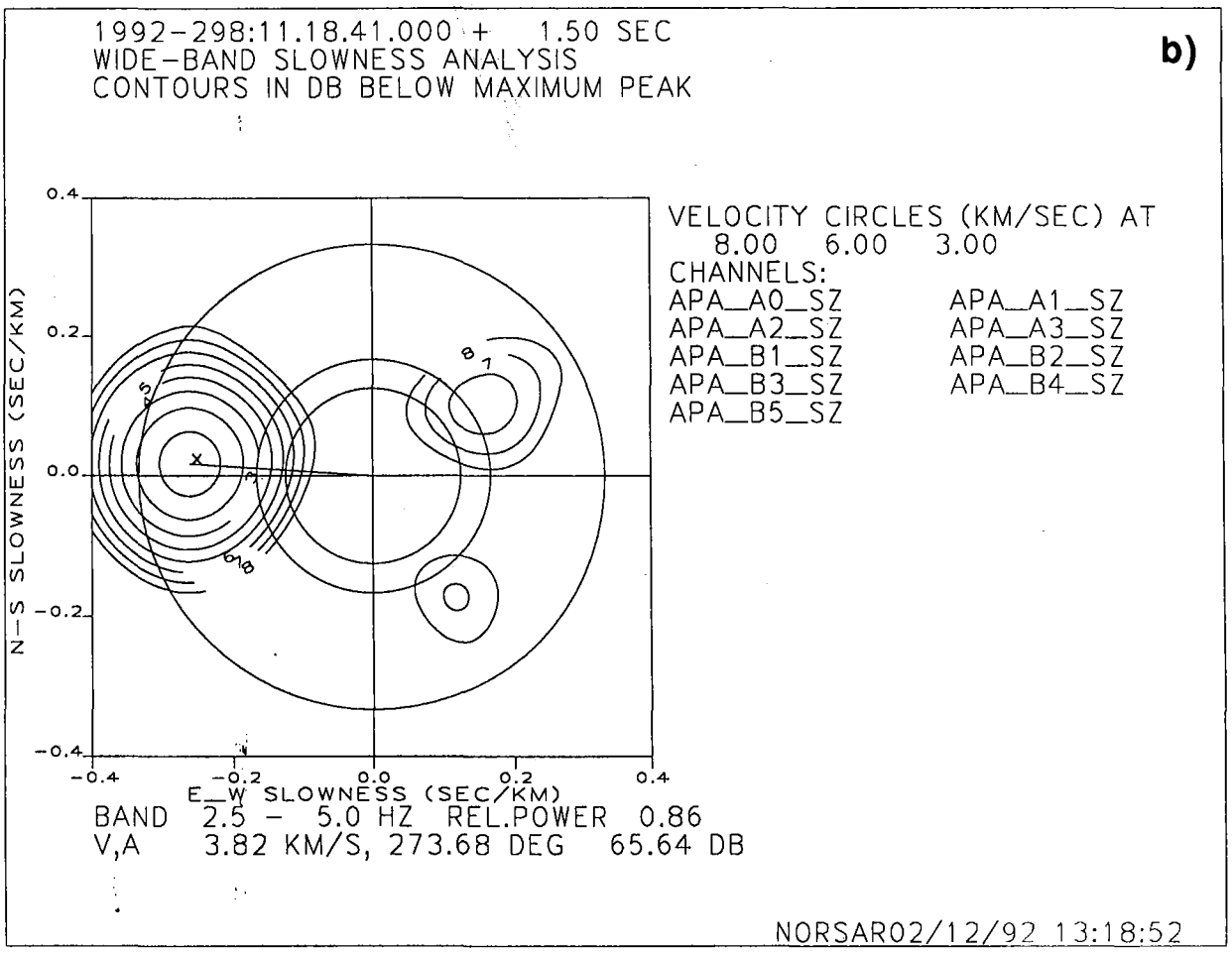

Fig. 7.2.5. (Page 2 of 3)

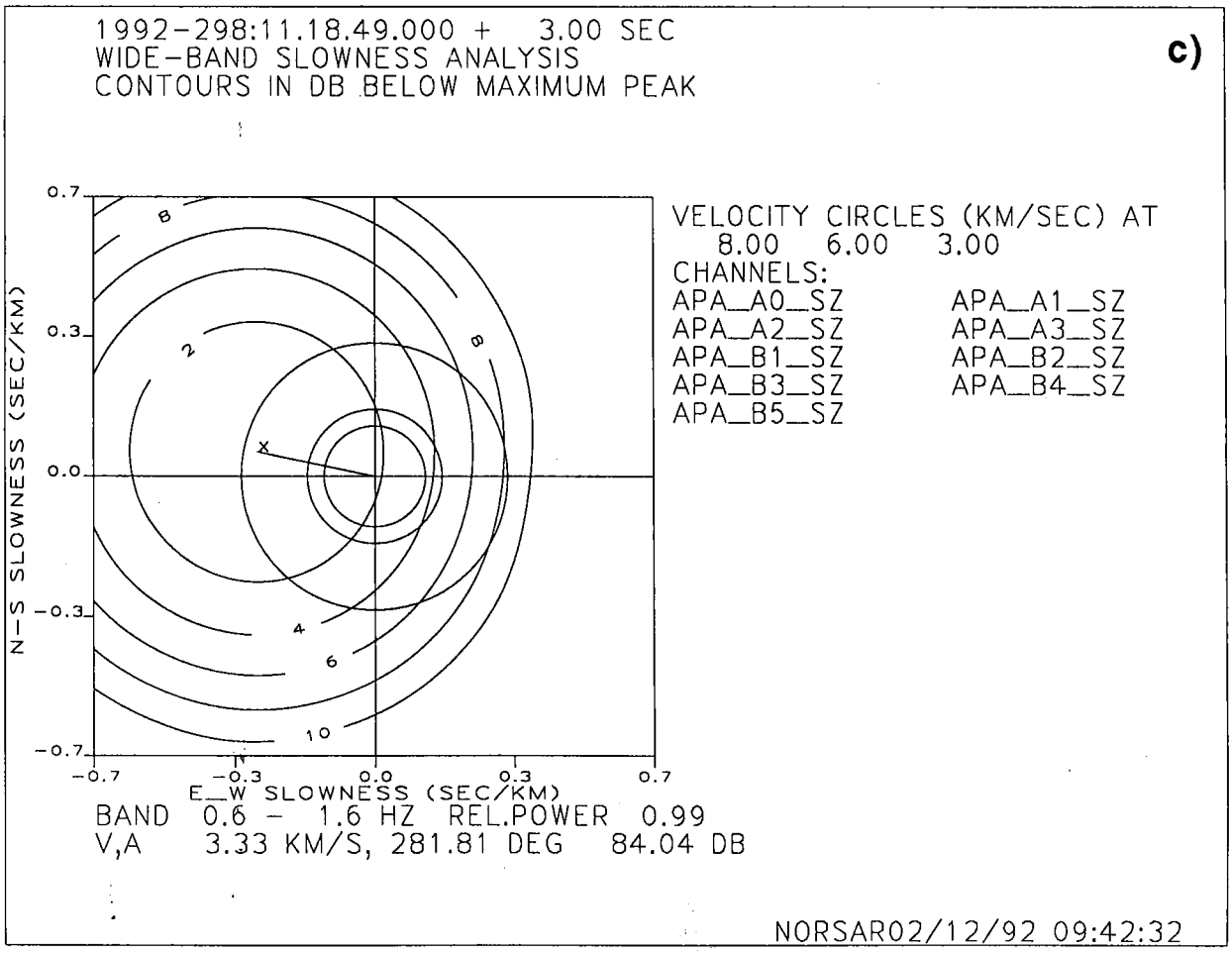

Fig 7.2.5. (Page 3 of 3)

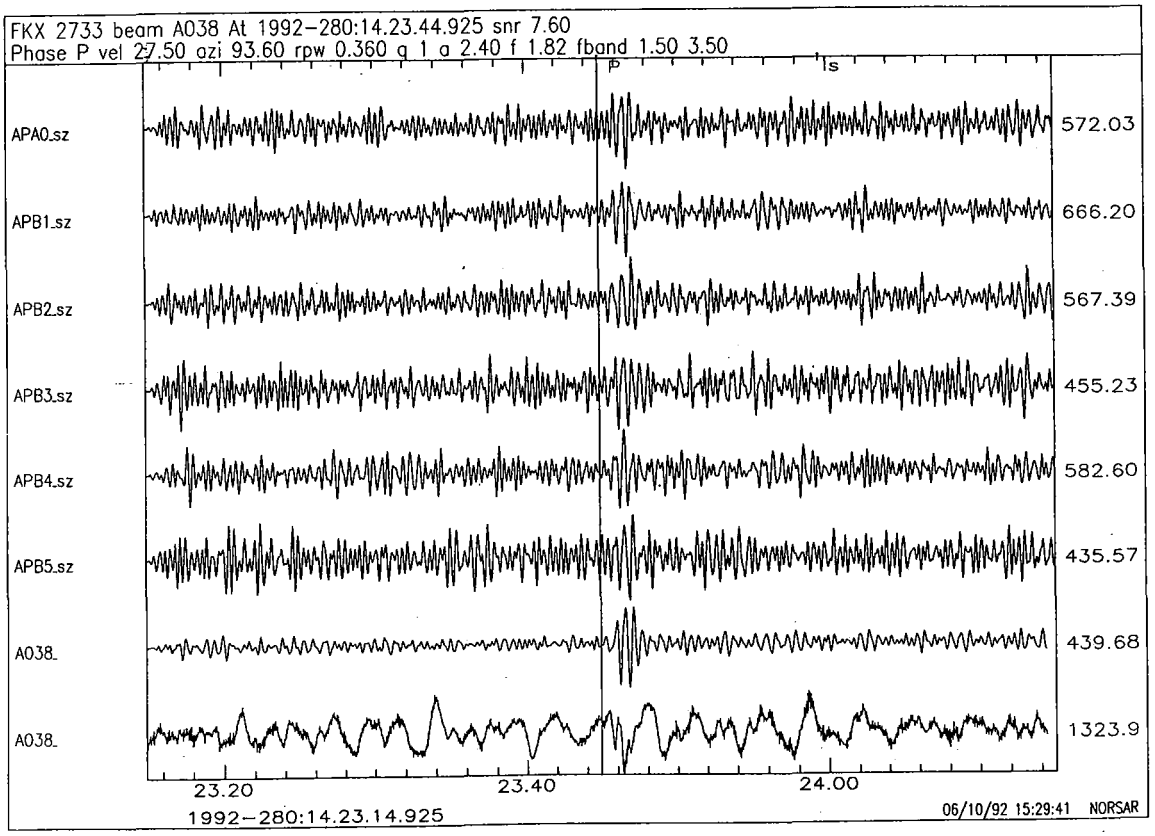

Fig. 7.2.6. Example of teleseismic event processing for the Apatity array. The top six traces are individual seismometer recordings, filtered in the band 1.5-3.5 Hz. The two bottom traces are array beams, filtered and unfiltered. Note the significant SNR improvement for the filtered array beam.